BBA - Molecular Basis of Disease 1865 (2019) 1502–1515

Contents lists available at ScienceDirect

BBA - Molecular Basis of Disease

journal homepage: www.elsevier.com/locate/bbadis

Mutation in NADPH oxidase 3 (NOX3) impairs SHH signaling and increases cerebellar neural stem/progenitor cell proliferation

P.C. Mazzonetto[a,1], C.B. Ariza[a,b,1], S.G. Ocanha[a], T.A. de Souza[c], G.M. Ko[a], C.F.M. Menck[c], S.M.G. Massironi[d], M.A. Porcionatto[a,*]

[a] Department of Biochemistry, Laboratory of Neurobiology, Escola Paulista de Medicina, Universidade Federal de São Paulo (UNIFESP), Brazil
[b] Department of General Pathology, Center of Biological Sciences, Universidade Estadual de Londrina (UEL), Brazil
[c] Department of Microbiology, Institute of Biomedical Sciences, Universidade de São Paulo (USP), Brazil
[d] Department of Immunology, Institute of Biomedical Sciences, Universidade de São Paulo (USP), Brazil

ARTICLE INFO

Keywords:
NADPH oxidase 3
Sonic hedgehog
Precursor/stem cell proliferation
Ataxia

ABSTRACT

Abnormalities in cerebellar structure and function may cause ataxia, a neurological dysfunction of motor coordination. In the course of the present study, we characterized a mutant mouse lineage with an ataxia-like phenotype. We localized the mutation on chromosome 17 and mapped it to position 1534 of the *Nox3* gene, resulting in p.Asn64Tyr change. The primary defect observed in *Nox3*^{eqlb} mice was increased proliferation of cerebellar granule cell precursors (GCPs). cDNA microarray comparing *Nox3*^{eqlb} and BALB/c neonatal cerebellum revealed changes in the expression of genes involved in the control of cell proliferation. *Nox3*^{eqlb} GCPs and NSC produce higher amounts of reactive oxygen species (ROS) and upregulate the expression of SHH target genes, such as *Gli1–3* and *Ccnd1* (CyclinD1). We hypothesize that this new mutation is responsible for an increase in proliferation *via* stimulation of the SHH pathway. We suggest this mutant mouse lineage as a new model to investigate the role of ROS in neuronal precursor cell proliferation.

1. Introduction

The cerebellum starts to develop at the embryonic phase and proceeds through the postnatal period, following cell-autonomous programs in combination with extracellular cues that direct proliferation, migration and cell fate specification [1]. Cerebellar neurons are born in the rhombic lip and ventricular zone at early stages of development (E10.5 in mice; week 9 in humans) [2], and continue to proliferate and migrate up to around postnatal day 15 (P15) in mice. Sonic hedgehog (SHH) expressed and secreted by Purkinje cells, starting at E16.5, is the main proliferative stimulus for granule cell precursor (GCP) proliferation [3]. SHH binding to Patched (PTCH) releases its inhibitory activity upon Smoothened (SMO), activating the SHH intracellular signaling pathway mediated by the GLI family of transcription factors [4].

Cerebellar functions include motor coordination and balance, and after it is fully developed, a relatively simple structure emerges, with a well-defined anatomy and physiology. The cytoarchitecture of the mature cerebellum is composed of eight neuronal types with distinct morphologies and location. In the adult cerebellum, connections between the main neurons are arranged in a stereotyped circuit that is repeated throughout its structure [1].

Abnormalities in cerebellar structure and function may cause ataxia, a neurological dysfunction of motor coordination that, in humans, can affect gaze, speech, gait, and balance [5]. Ataxia may arise due to very different causes, such as tumors, genetic factors, drug toxicity, and metabolic dysfunction. Hereditary ataxia, which is relevant to humans, can be divided into two groups, *i.e.* autosomal recessive ataxia, and autosomal dominant spinocerebellar ataxia [5].

In the course of the present study, we characterized a mutant mouse lineage that displays an ataxia-like phenotype. The primary phenotypic characteristic we observed was lack of motor coordination, attributed to increased proliferation of cerebellar GCPs. Through genetic analysis, followed by exome DNA sequencing, we localized the mutation to NADPH oxidase 3 (NOX3), in a position not previously described [6], and investigated how increased production of reactive oxygen species (ROS) may affect proliferation through stimulation of SHH signaling pathway. We suggest that this new mutant mouse lineage is a fascinating model to investigate ataxia, as well as to examine the role of ROS in the control of neuronal precursor proliferation and may help to identify new types of human cerebellar ataxias.

* Corresponding author.
E-mail address: marimelia.porcionatto@unifesp.br (M.A. Porcionatto).
[1] These authors contributed equally to this work.

https://doi.org/10.1016/j.bbadis.2019.02.022
Received 8 August 2018; Received in revised form 25 February 2019; Accepted 27 February 2019
Available online 08 March 2019
0925-4439/

2. Methods

2.1. Mice

The recessive mutation *Nox3*^{eqlb} is maintained in a BALB/c background [7]. The mutants do not have fertility problems, although they present a larger interval between pregnancies, and slightly smaller litters when compared to wild-type BALB/c. Mice were maintained in an Animal Care Facility under specific pathogen-free (SPF) conditions, fed a standard laboratory diet and water *at libitum*. Mice were kept at 20 ± 2 °C with 12 h light/dark cycle and relative humidity of 60%. All experiments were carried out in accordance with the guidelines of ILAR (Institute of Laboratory Animal Research) and were approved by the Ethics in Research Committee of Federal University of São Paulo (UNIFESP; CEP 1629/05 and CEUA 7896100815). All efforts were made to minimize animal suffering and to reduce the number of animals used.

2.2. Breeding and genetic mapping

F1 mice were generated by crossing *Nox3*^{eqlb} (BALB/c background) mice with C57BL/6 mice. F2 generation was produced by F1 brother-sister mating. Mutant mice were identified by their body position when hung by the tail according to the same parameters used to select *Nox3*^{eqlb} mice [7]. To assign chromosomal linkage, DNA was obtained from the tails, spleen or kidney of a set of 190 F2 mice. Tissues were digested by incubation with 20 mg/ml Proteinase K (Invitrogen, Carlsbad, US) for 1 h at 65 °C. DNA was used to perform linkage analysis by Single Sequence Length Polymorphism (SSLP), also called microsatellites, detected by Polymerase Chain Reaction (PCR). PCR were performed using 100 ng DNA and Taq polymerase (Invitrogen). Amplification products were analyzed by 10% polyacrylamide electrophoresis and were visualized by silver staining. Linkage analysis was performed manually, by looking for divergence from the expected Mendelian proportions.

2.3. Exome sequencing

Genomic DNA was extracted from small tail biopsies (1–2 mm) of male mice using a Macherey-Nagel Genomic DNA from Tissue kit (Macherey-Nagel, Düren, Germany) with RNase treatment. DNA was quantified using the Qubit 2.0 (Life Technologies, Carlsbad, US) and quality was evaluated both by agarose gel electrophoresis and by the Nanodrop-1000 (Wilmington, DE, US). Exome enrichment was performed using the SureSelect Mouse All-Exon Kit (Agilent Technologies, Santa Clara, US) following the manufacturer protocols. Libraries were evaluated electrophoretically with an Agilent Bioanalyzer 2100 (Santa Clara, US). Prepared exome libraries were pooled and subjected to emulsion PCR and sequenced on the 5500xl SOLiD Genetic Analyzer (Life Technologies) as single-end 75-bp reads at the Core Facility for Scientific Research – University of Sao Paulo (CEFAP–USP/GENIAL).

2.4. Read mapping, variant calling and SNV filtering

Reads obtained both for *Nox3*^{eqlb} and BALB/c samples were mapped to the reference mouse genome (mm9/NCBI37) with Lifescope Genome Analysis Software v2.5.1 (Life Technologies) using default targeted-resequencing parameters. Raw SNVs were called by the diBayes algorithm (Life Technologies) with no both-strand allele requirement. SNV filtering strategy was adapted from Fairfield et al. [8]. The strategy was developed based on chromosomal regions obtained by meiotic genetic mapping; mode of inheritance (ratio of alleles for a homozygous SNV > 0.65 for variant allele); absence on control BALB/c sample; novelty when compared to NCBI dbSNP build 128; annotation as non-synonymous changes or laying in potential splicing-donor-sites; uniqueness when compared to unrelated mouse exome datasets. Sex-averaged cM were converted to base pairs using Jax Mouse Map Converter [9]. VCFTools [10] was used for SNV data manipulation and all annotation steps were performed using ANNOVAR [11]. Alignments were visualized with Integrated Genome Viewer (Broad Institute).

2.5. In-silico evaluation of candidate SNVs

Predictions of functional effects of candidate SNVs were performed using three different softwares, *i.e.* Sorting Intolerant From Tolerant Amino Acid Substitutions (SIFT) ([53]), Protein Variation Effect Analyzer (PROVEAN) [12] and Polymorphism Phenotyping v.2 (PolyPhen-2) [13]. SIFT prediction scores < 0.05 were classified as being damaging and PROVEAN predicts amino acid substitutions as deleterious if its score is less than the −2.5 cutoff. PolyPhen-2 classifies a substitution as “probably damaging” only if its score is larger than 0.85. Both protein sequences of 568aa (NP_945196.2, ENSMUSP00000111466) of mouse NADPH oxidase 3 (Nox3) were used for predictions.

2.6. SNV validation

Candidate SNV was validated by Sanger sequencing. Briefly, genomic DNA from *Nox3*^{eqlb} and unaffected control inbred mice (BALB/c, C57Bl/6, 129, CH3 and NZW) was amplified by conventional PCR using PCR Master Mix (Promega, Madison, US) and primers designed around the location in exon 3 of *Nox3* gene (Table 1). Amplicons were bidirectionally sequenced using Big Dye Terminator version 3.1 Cycle Sequencing Kit (Applied Biosystems, Foster City, CA) on ABI Prism 377 DNA sequencer (Applied Biosystems). Chromatogram analysis was conducted using Geneious 6.1.6 (Biomatters Limited, Auckland, New Zealand).

2.7. PCR-RFLP

DNA from BALB/c and *Nox3*^{eqlb} was amplified by conventional PCR using PCR Master Mix (Promega) and *Nox3* primers (Table 1). The amplification product was digested by Tru1l (Msel) (Thermo Fisher Scientific, Waltham, US) at 65 °C for 1 h on Eppendorf Mastercycler® Personal (Applied Biosystems), according to the manufacturer orientation. The restriction fragments generated by Tru1l were analyzed by 10% polyacrylamide gel electrophoresis.

2.8. Motor coordination analysis

2.8.1. Rotarod test

The apparatus was built by the Biomedical Engineering Department of UNIFESP based on commercially available Rotarods, and consists of a base platform and a rotating bar with a diameter of 2.5 cm. The rotating bar was placed at a height of 13 cm from the base. Rotarod performance test evaluated 39 mice (19 *Nox3*^{eqlb}; 20 BALB/c) using the speed of 7 rpm. Balance performance was assessed based on the time of permanence of each animal on the rod over a 30 s period, according to the formula $Pt_{(s)} = 30 / (\#\ of\ falls + 1)$.

2.8.2. Rotarod training

A total of 45 mice (23 *Nox3*^{eqlb}; 22 BALB/c) were trained under continuous speed of 7 rpm in 5 minute sessions, three times a week. After two weeks of training, mice were tested and balance perform was assessed based on the permanence time on the rod, as described above.

2.9. Preparation of tissue sections for immunohistochemistry

Tissue sections were obtained from BALB/c and *Nox3*^{eqlb} mice brain at postnatal ages P3, P6, P9, P12, P15 and adult (> P30). Animals with age up to P15 were decapitated without any anesthesia and adults are deeply anesthetized with ketamine/xylazine (i.p.), followed by intracardiac perfusion of 0.9% saline solution, pH 7.4, followed by 4%

Table 1
Primers sequences used for qPCR analysis.

Genes	Primer sequence (5′-3′)	Product (bp)
Actb	FWR: CCTAAGGCCAACCGTGAAAA REV: GTGGTACGACCAGAGGCAT	113 bp
Akt1	FWR: CCTCTGCTTTGTCATGGAGTAT REV: CACAATCTCCGCACCATAGAA	109 bp
Ccna	FWR: CACTGACACCTCTTGACTATCC REV: TGGCTGCCTCTTCATGTAAC	191 bp
Ccnb1	FWR: CTGACCCAAACCTCTGTAGTG REV: CTTCACGACCCTGTAGGTATTT	105 bp
Ccnd1	FWR: GATGAAGGAGACCATTCCCTTG REV: TCACCAGAAGCAGTTCCATTT	101 bp
Cd133	FWR: TGGCATTCTGTGTGGCTATGTTGC REV: TGCGATAGTACTTGGCCAGCTTGA	122 bp
Cdc25	FWR: CTGAAAGAAGAGTCCGAGGATG REV: GAGAGAGTGCTGCGGTTATT	194 bp
Cdk1	FWR: CGGTTGACATCTGGAGCATA REV: GCATTTTCGAGAGCAAGTCC	100 bp
Cdk2	FWR: CGGAGCTTGTTATCGCAAATG REV: CATCCTGGAAGAAAGGGTGAG	88 bp
Cdkn2a	FWR: ACCGAACTGGTTTTGCTGTC REV: GGGCAGGTTCCCTTCATTAT	106 bp
Duox1	FWR: AGCTACAAAGGGCTGAAGATG REV: CCCTGGCTTTGGTGTAAGAA	198 bp
Duox2	FWR: AGCTATGCCCTCATCCAATTAC REV: CACCCACTGCCCTGATTT	201 bp
Gapdh	FWR: ACCCAGAAGACTGTGGATGG REV: ACACATTGGGGGTAGGAACA	172 bp
Gli1	FWR: CCTGTGTACCACATGACTCTAC REV: GCACTTGCCAACCATCATATC	113 bp
Gli2	FWR: CTCGACCTACAACGCATGATT REV: CCAGCAGACAGATGTCCATAAG	110 bp
Gli3	FWR: CCAGCAGACAGATGTCCATAAG REV: GTCAGCCACACTCACATTCT	139 bp
Hprt	FWR: CTCATGGACTGATTATGGACAGGA REV: GCAGGTCAGCAAAGAACTTATAGCC	123 bp
Nox1	FWR: CTCCCTTTGCTTCCATCTTGA REV: AGTGAGGAAGAGACGGTAGTT	203 bp
Nox2	FWR: AGTGCCCAGTACCAAAGTTC REV: CCTCCATCTTGAATCCCTTCTT	195 bp
Nox3	FWR: GCTGAGCAAGGTGTACTTCTAT REV: CCAGACTTTCATCCCAGTGTAA	194 bp
Nox3[a]	FWR: CTGGCAGTAAACGCCTATCT REV: AGCACACACTTGTTCCTCTC	312 bp
Nox4	FWR: GGTGGTATTGTTCCTCATGGT REV: TTCTGGGATGATGTCTGGTTAAG	204 bp
Noxo1	FWR: CTGCTACGGAGATCTGAACAAG REV: ATCCAGAGGTTTGGGTACAAAG	192 bp
Rb1	FWR: CTTTACTGGCCTGTGCTCTT REV: ATCCACGGGAAGGACAAATC	97 bp
Rplp0	FWR: CCTCCTTCTTCCAGGCTTTG REV: CCACCTTGTCTCCAGTCTTTATC	99 bp
Sox2	FWR: ATGCACAACTCGGAGATCAG REV: TTTATAATCCGGGTGCTCCTTC	132 bp

FWR - forward; REV - reverse.
[a] Sequence used for Sanger sequencing and PCR-RFLP assay.

paraformaldehyde (PFA) in 0.1 M PBS, pH 7.4. The brains were removed from the skull, post-fixed overnight at room temperature in the same fixative, and cryoprotected in 0.1 M PBS, pH 7.4, containing 30% sucrose. Brains were frozen in isopentane (Sigma-Aldrich Corporation, St. Louis, US) using dry ice and embedded in Tissue Tek (Electron Microscopy Sciences, Hatfield, PA). Cryostat midsagittal sections (20 µm thickness) were mounted on glass silanized slides (DakoCytomation, Ely, United Kingdom).

2.10. Immunohistochemistry for calbindin

Brain sagittal sections were permeabilized by incubation with 0.1% Triton X-100 in PBS for 1 h and non-specific sites were blocked by incubation in 10% bovine serum albumin (BSA) (Cultilab, Campinas, Brazil) for 1 h at room temperature. Following the blocking period, sections were incubated with anti-calbindin (rabbit anti-calbindin D-28K, CHEMICOM, Temecula, US) 1:100 in blocking solution (10% BSA, 0.1% Triton X-100) overnight at 4 °C. After, brain sections were incubated in anti-rabbit conjugated with Alexa Fluor®-488 and in DAPI (*4′-6-diamidino-2-phenylindole*; Sigma) solution (100 ng/ml in 0.1% Triton X-100 in PBS) for 1 h at room temperature in dark. Images were captured using a Nikon Eclipse E600 microscope (Media Cybernetics, Silver Spring, US).

2.11. Evaluation of GCPs migration in vivo

Postnatal littermates of BALB/c and *Nox3*^{eqlb} at day 5 were injected intraperitoneally with 50 mg/kg body weight BrdU (Sigma) diluted in PBS and were decapitated 24, 48, 72 and 96 h later (at P6, P7, P8 and P9). Brains sagittal sections were permeabilized by incubation with 0.1% Triton X-100 in PBS for 1 h and non-specific epitopes were blocked by incubation with 10% BSA (Cultilab) for 1 h at room temperature. Sagittal sections were treated with 2 N HCl at 37 °C for 30 min and were incubated for 1 h with anti-BrdU conjugated with Alexa Fluor®-594 (Molecular Probes, Eugene, US) 1:100 in blocking solution (10% BSA, 0.1% Triton X-100) overnight at 4 °C in dark. After, sections were incubated with DAPI (*4′-6-diamidino-2-phenylindole*; Sigma) solution (100 ng/ml in 0.1% Triton X-100 in PBS) for 1 h at room temperature in dark. Images were captured using a Nikon Eclipse E600 microscope (Media Cybernetics).

2.12. Proliferation assay

Proliferation of granule cell precursors was assessed by [^{3}H]-thymidine (Amersham/GE Healthcare UK Ltd, Little Chalfont, England) incorporation using organotypic culture and isolated granule cell culture, as previously described [14]. Cultures were incubated with [methyl-^{3}H]-thymidine (0.25 µCi/ml) and were washed with 5% TCA. After incubation with 0.5 N NaOH for 1 h at 37 °C, the extract was added to Ultima-Gold™ (Packard Instruments Company Inc., Downers Grove, US) scintillation liquid and incorporated [^{3}H]-thymidine was measured by a Liquid Scintillation Analyzer – TRI-CARB 2100TR (Packard Instruments Company Inc., Downers Grove, US).

2.13. Organotypic culture

Briefly, P3, P6, P9, P12 and P15 mice (BALB/c and *Nox3*^{eqlb}) cerebella were dissected and sagittal sections (200 µm thick) were cut using a vibrating microtome (Vibratome, St. Louis, US). Slices were incubated in DMEM/F12 1:1 medium (Invitrogen) containing 24 mM KCl, 36 mM glucose, 15 mM HEPES, 10% fetal bovine serum (FBS, Cultilab) and 10% penicillin/streptomycin (ICN Biomedicals Inc., Irvine, CA) with 0.5 µCi/ml of [^{3}H]-thymidine (Amersham/GE Healthcare) in a humidified incubator at 37 °C with 5% CO_2. After 24 h in culture, thymidine incorporation was evaluated. Each experiment was repeated three times with a total of 8–10 slices/animal, 6–7 animals per age. The results are mean value of all slices used in each experiment.

2.14. GCPs culture

Primary cultures of granule cell precursor from P6 mouse cerebellum were established as previously described [15]. GCP were cultured in DMEM/F12 1:1 medium (Gibco, Gaithersburg, US) containing 10% FBS (Cultilab), 20 mM KCl, 1% glutamine (Sigma) and 1% penicillin/streptomycin, in a humidified incubator at 37 °C with 5% CO_2.

2.15. NSCs culture

Primary cultures of cerebellar neural stem cell were isolated from P6 mice cerebellum as previously described [16]. Briefly, NSC were cultured as neurospheres in Neurobasal® medium (Gibco) containing

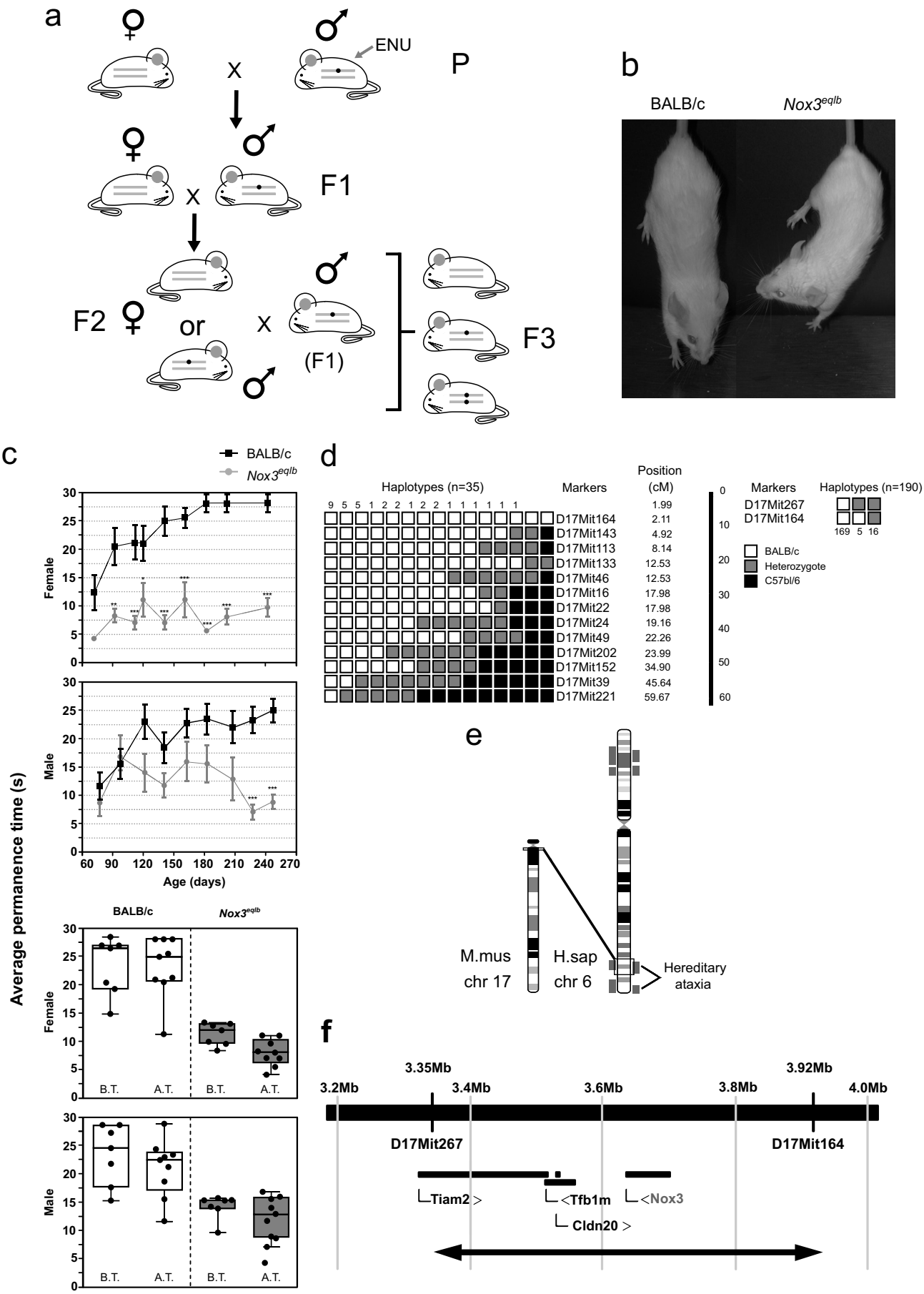

(caption on next page)

Fig. 1. Phenotypic characterization of *Nox3*^{eqlb} mouse and genetic mapping of the mutation.
(a) For linkage analysis, BALB/c mice homozygous for the mutant allele were crossed to C57BL/6, and +/*Nox3*^{eqlb} heterozygous F1 were intercrossed for the production of an F2 with homozygous recessive phenotypes.
(b) Wild-type BALB/c (WT) shows normal body position when held by the tail; *Nox3*^{eqlb} mouse twists upwards.
(c) BALB/c and *Nox3*^{eqlb} mice were tested on the rotarod. The average permanence time at 7 rpm was measured. N = 20 BALB/c: 10♂ and 10♀; 19 *Nox3*^{eqlb}: 11 ♂ and 8♀. Black line: BALB/c; gray line: *Nox3*^{eqlb} (**p < 0.01; ***p < 0.0001). (b′) Fifteen days of training did not improve mice performance on rotarod. N = 22 BALB/c: 11♂ and 11♀; 23 *Nox3*^{eqlb}: 11♂ and 12♀.
(d) Haplotype representing 190 mice and polymorphic markers used to locate *Nox3*^{eqlb} mutation between D17Mit164 and D17Mit267 markers. N = 169 BALB/c (white squares), 5 Heterozygotes (BALB/c and C57bl/6; gray squares) and 16 C57bl/6 (black squares).
(e) Region of *Nox3*^{eqlb} mutation syntenic to human chromosome 6 indicating several mapped recessive ataxia loci.
(f) Genes located between markers D17Mit267 and D17Mit164 in mouse chromosome 17: *Tiam2* (T-Cell Lymphoma Invasion and Metastasis 2), *Tfb1m* (Transcription Factor B1, Mitochondrial), *Cldn20* (Claudin 20) and *Nox3* (NADPH oxidase 3).

2% B27 supplement (Gibco), 20 ng/ml EGF (Sigma), 20 ng/ml FGF2 (R &D Systems, Minneapolis, US), 1% penicillin/streptomycin and 1% glutamine (Sigma), in a humidified incubator at 37 °C with 5% CO_2. To perform proliferation assay after apocynin treatment *in vitro* and to measure endogenous ROS, the neurospheres were dissociated with 0,25% trypsin and 1 mM EDTA.

2.16. Apoptosis assay

Terminal deoxynucleotidyl transferase (TdT)–mediated dUTP nick and labeling (TUNEL) staining was performed in accordance to the manufacturer's instructions of the ApopTag *in situ* Apoptosis Kit Detection (CHEMICOM, Temecula, CA). Briefly, sections were incubated with TdT enzyme in a humidified chamber for 1 h at 37 °C and incubated with anti-digoxigenin conjugate in a humidified chamber for 30 min in the dark at room temperature. Finally, sections were incubated with 100 ng/ml DAPI in PBS for 1 h at room temperature. Images were captured using a Nikon Eclipse E600 microscope (Media Cybernetics).

2.17. RT-PCR and qPCR

Total RNA was extracted from P6 mice cerebella using Trizol (Invitrogen) according to the manufacturer's instructions and quantified using the spectrophotometer NanoVue Plus (GE Healthcare). Total RNA (2 µg) was used to produce cDNA using ImProm-II™ Reverse Transcription System (Promega) and Recombinant RNasin® Ribonuclease inhibitor (Promega). qPCR was performed using 10 ng cDNA and Sybr® Master Mix (Applied System) in 7500 Fast Real-Time PCR System (Applied Systems). Relative quantitation of gene expression was calculated using the $2^{-\Delta\Delta Ct}$ method and normalized to previously characterized reference genes [17]. The primer sequences are listed in Table 1.

2.18. Microarray analysis

For the analysis of differential gene expression between the *Nox3*^{eqlb} and BALB/c, RNA was extracted from mice with 6 and 15 days postnatal. Data were analyzed using the software ArrayStar, using the normalization standard RMA (robust multi-array average) and the differentially expressed transcripts were identified using Student's *t*-test, including correction of Benjamini-Hochberg MTC (Multiple Testing Corrections; Allison, Cui, et al. [54]) with $p < 0.05$ and fold change ≥ 1.5. A file containing the GenBank accession number, the value of fold change and p values with the Benjamini-Hochberg correction MTC was submitted to the IPA software (Ingenuity Pathway Analysis, Ingenuity Systems, Inc., Redwood City, US, http://www.ingenuity.com/).

2.19. Measuring endogenous ROS levels

Approximately 4.7×10^5 per well of cerebellar NSC and 4.0×10^4 per well of cerebellar GCP were plated in a dark plate pre-coated with poly-L-lysine (Sigma-Aldrich). Intracellular production of ROS was measured in cerebellar GCP and NSC after 7 and 12 days *in vitro* by 100 µM DCFH-DA to determine H_2O_2 generation. Fluorescence was detected using Victor-3TM Multilabel Counter (PerkinElmer, Waltham, US) with excitation at 490 nm and emission at 535 nm.

2.20. Apocynin treatment in vitro

Cerebellar GCP and NSC were plated at a density of 2×10^4 per well in pre-coated plate with poly-L-lysine (Sigma) to promote GCP adhesion or pre-coated plate with Poly-HEMA (Sigma) to prevent NSC cell adhesion and differentiation. After 7 days in culture, GCP and NSC were treated with 100 µM apocynin or 1% DMSO for 24 h. The CellTiter 96® AQ_{ueous} One Solution Cell Proliferation Assay kit (Promega) was used according to the manufacturer's instructions. Briefly, 20 µl of the MTS reagent was added into each well and cells were incubated at 37 °C for 2 h in the dark. The absorbance was detected at 490 nm using SpectraMax® M3 Multi-Mode Microplate Reader (Molecular Devices, Sunnyvale, US).

2.21. Apocynin treatment in vivo

Pups from BALB/c and *Nox3*^{eqlb} mice (P2 to P8) were treated with NADPH-oxidase inhibitor 10 µg/g apocynin (Sigma-Aldrich; 4-hydroxy-3-methoxy-acetophenone) or 0,2% DMSO (R&D Systems; dimethyl sulfoxide), administered intraperitoneally (i.p.) daily. After 24 h, mice were anesthetized with sodium thiopental and transcardially perfused with 4% paraformaldehyde. Free-floating brain sagittal sections obtained in a cryostat CM 1850 (Leica Instruments GmbH, Heidelberg, Germany) were permeabilized by incubation with 0.1% Triton X-100 in PBS for 10 min and non-specific sites were blocked by incubation in 10% FBS (Cultilab) for 1 h. The sections were incubated in DAPI (*4′-6-diamidino-2-phenylindole*; Sigma) solution (100 ng/ml in 0.1% Triton X-100 in PBS) for 1 h at room temperature in the dark. Images were captured by confocal microscopy using Zeiss Axio Observer Z1 (Carl Zeiss, Oberkochen, Germany) and analyzed by ImageJ® software using straight tool.

3. Results

3.1. Mapping Nox3^{eqlb} mutation

In the course of a recessive ENU mutagenesis screening in BALB/c mice (Fig. 1a), we established a colony of mice bearing poor motor coordination and balance [7]. The phenotypic features that allowed for the selection of the mutant mouse *Nox3*^{eqlb}, originally called *eqlb* (equilibrio, “balance” in Portuguese) were a downward posture reflex when hung by the tail (Fig. 1b) and poor performance in the rotarod test (Fig. 1c; Supplementary video). The combination of lack of motor coordination and balance was not due to degeneration as the phenotype did not worsen with age, and could not be corrected by training (Fig. 1c). Body development was not impaired by the mutation, and weight gain curves were similar to BALB/c, as was the average number

of pups per litter, although the interval between births was significantly higher in the mutant (Supplementary Fig. 1).

We performed linkage analysis to map the mutation using 190 mice from F2 mutant offspring of an intercross between mutant BALB/c (*Nox3*^{eqlb}) males and C57BL/6 wild type females. The analysis located the mutation to chromosome 17, within a 0.12 cM (~0.57 Mb) interval flanked by the markers D17Mit164 and D17Mit267 (Fig. 1d), a region syntenic to a region in human chromosome 6 in which several ataxia markers have been mapped (Fig. 1e). Candidate genes present in the region of the mutation are *Tiam2*, *Tfb1m*, *Cldn20* and *Nox3* (Fig. 1f).

a

Analysis of SNV filtering strategy from *Nox3*^{eqlb} exome sequecing

	Inheritance	Mapped Region	Overlap with mapped region	Homozygous[a]	Exclusive Mutations	Not in dbSNP[b]	Non-synonymous, splice sites	Unique[c]	Candidate	Local coverage
Nox3^{eqlb}	Recessive	Chr.17:up to 10 cM	212	185	16	7	1	1	Nox3, exon 3; c.A250T.p.N64Y	115X

[a] >0.65 allelic ratio for variant allele. [b]Compared to dbsnp128. [c]Compared to unrelated exome datasets.

b

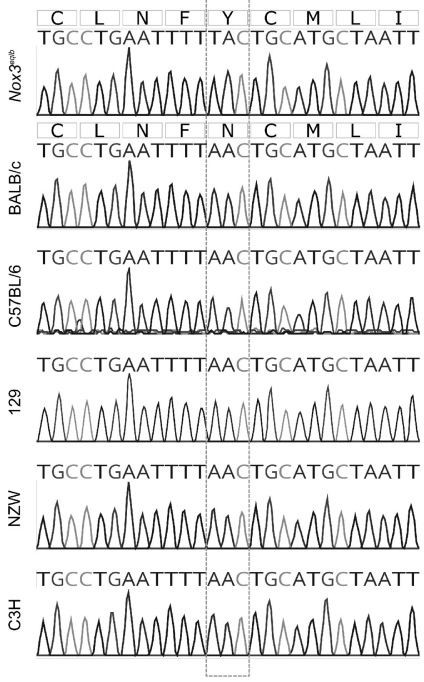

c

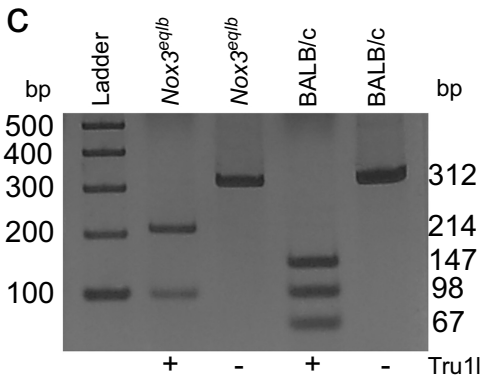

d

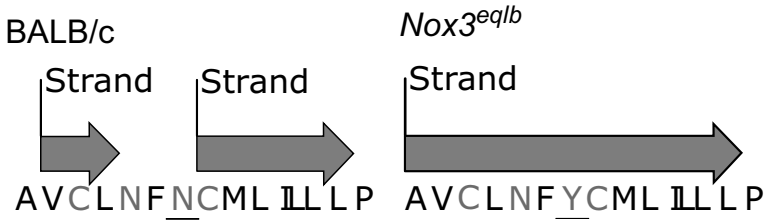

e

Prediction of functional effects of *Nox3*^{eqlb} mutant allele on NOX3 protein variants

Acession number	Protein variant	Correspondent substitution	SIFT prediction	PROVEAN prediction	PlyPhen-2 prediction
ENSMUSP00000111466	Nox3 (568aa)	N64Y	Damaging	Deleterious	Probably damaging

f

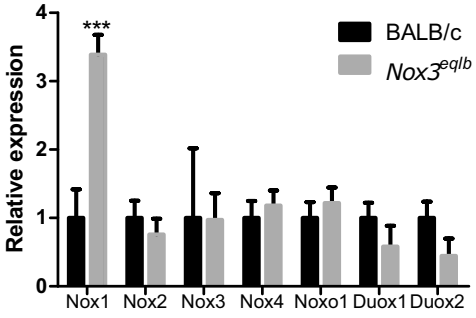

g

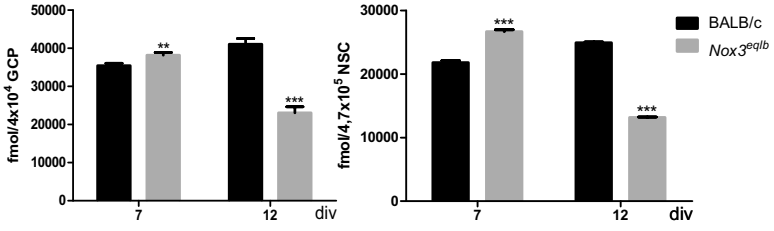

(caption on next page)

Fig. 2. Asp 64 is substituted by Tyr 64 in *Nox3*^{eqlb}.
(a) Analysis of SNV filtering strategy from *Nox3*^{eqlb} exome sequencing.
(b) Sanger sequencing of exon 3 of *Nox3*. *Nox3*^{eqlb} mouse shows an A to T transversion in *Nox3* with amino acid change from asparagine (N) to tyrosine (Y) at position 64. Analysis and image generated by Geneious Software 6.1.6.
(c) PCR-RFLP assay of DNA from *Nox3*^{eqlb} and BALB/c mice using Tru1l restriction enzyme (lanes indicated by *). The analysis by 10% polyacrylamide gel electrophoresis shows two products for *Nox3*^{eqlb} and three for BALB/c.
(d) Prediction analysis for NOX3 protein shows one beta strand in *Nox3*^{eqlb} rather than two beta strands in BALB/c in the sequence between Ala 58 and Pro 71.
(e) Impact predictions of the SNV on NOX3 function.
(f) *Nox1* expression is upregulated in the cerebellum of P6 *Nox3*^{eqlb} when compared to BALB/c. Data normalized to *Gapdh* expression. N = 3 *Nox3*^{eqlb} cerebella; N = 3 BALB/c cerebella (***$p < 0.001$).
(g) Quantification of H_2O_2 production by cerebellar granule cell precursors (GCPs) and neural stem cells (NSCs) after 7 and 12 days *in vitro* (DIV) using DCFH-DA (100 μM). N = 36 wells (GCPs, 7 DIV); N = 25 wells (GCPs, 12 DIV); N = 6 wells (NSCs, 7 DIV); N = 4 wells (NSCs, 12 DIV). Representative data from one experiment repeated three times. (**$p < 0.01$; ***$p <$ 0,0001).

Exome sequencing of DNA extracted from the mutant mice provided approximately 62 M reads of 75 bp (approx. 4.6 Gb) of which > 92% were mapped on mm9/NCBI37 mouse reference genome. Capture efficiency was high: > 81% of reads were mapped on target regions and > 94% of targeted bases were covered at least once. The average depth of coverage within targets was approximately 44-fold with > 88% of target bases covered at least 10 times. Exome sequencing of control BALB/c provided similar results, with a higher average depth of coverage within targets (data not shown). The mouse reference genome is mainly from the C57BL/6 inbred strain; thus, the raw number of SNPs was > 70,000 even in the unaffected BALB/c control mouse exome dataset. We therefore applied a singular nucleotide variants (SNVs) filtering strategy in order to reduce the number of SNVs based on the linkage map, restricted up to 10 cM of chromosome 17, where the mutation was mapped (Fig. 1d). Because of the recessive Mendelian inheritance of the mutant phenotype, we eliminated heterozygous SNV callings. After that, 185 homozygous SNV in the mapped region remained (Fig. 2a). Those SNVs were compared to SNVs called in the control BALB/c mouse sequenced and only 8.6% of them were exclusive to the mutant. Among them, after dbSNP filtering, annotation and comparisons among unrelated exome datasets, we were able to select only one SNV in exon 3 of *Nox3* gene (accession number ENSMUSP00000111466). This SNV is a 115× covered T to A transversion at 3695328 bp of chromosome 17, which implies a non-synonymous A to T change in the coding sequence and an asparagine (Asn) to tyrosine (Tyr) exchange in the amino acid sequence (Fig. 2a). We validated this SNV by Sanger sequencing covering exon 3 of *Nox3*, in the region flanked by the markers D17Mit164 and D17Mit267 (Fig. 2b). We compared the mutant sequence with other unrelated inbred strains (NZW, 129, C3H and C57BL/6) and confirmed that this sequence mutation was unique to the mutant and was not a polymorphism. We then renamed the mutant *Nox3*^{eqlb} following the Jackson Laboratory Guidelines (https://www.jax.org/jax-mice-and-services/customer-support/technical-support/genetics-and-nomenclature).

In silico analysis predicted that A > T transversion caused the removal of a restriction site for Tru1I in exon 3. To verify this, we amplified a sequence flanked by the same primers used for Sanger sequencing (Table 1) using genomic DNA from BALB/c and *Nox3*^{eqlb}, digested the products with Tru1l and analyzed by electrophoresis. As predicted, we observe three restriction fragments originated from BALB/c DNA digestion (67, 98 and 147 bp) and two fragments from *Nox3*^{eqlb} DNA (98 and 214 bp) (Fig. 2c). Additionally, *in silico* prediction analysis also indicated the conversion of two proximal beta strands in one in the segment comprehended between amino acids 58 and 71 (BALB/c AVCLNF**N**CMLILLP; *Nox3*^{eqlb} AVCLNF**Y**CMLILLP) (Fig. 2d).

To gain insights into the effects of this new *Nox3* allele, we performed impact predictions of SNV on NOX3 and found it to be deleterious/damaging, indicating that the Asn to Tyr substitution implies in significant changes in protein structure and function (Fig. 2e). Next, we quantified the expression of the *Nox* family members *Nox1–4*, *Duox1–2* and NADPH oxidase organizer (*Noxo1*) by qPCR, searching for compensatory gene expression. We found that *Nox1* expression was upregulated in *Nox3*^{eqlb} mutant cerebellum, whereas expression of *Nox3* did not change (Fig. 2f). These results led us to further investigate the relationship between the genotype and the ataxic phenotype of *Nox3*^{eqlb}.

3.2. Mutation in Nox3 causes increased ROS production by cerebellar GCPs and neural stem cells (NSCs)

NOX-derived ROS are involved in many cellular events in the nervous system, and high levels of ROS are linked to the self-renewal capacity, multipotency, and proliferation of neural stem and progenitor cells [18]. In order to investigate if ROS production by cerebellar GCPs and NSCs would be affected by *Nox3*^{eqlb} mutation, we cultured both cell types derived from *Nox3*^{eqlb} and BALB/c cerebella for 7 and 12 days, and measured intracellular ROS. Interestingly, *Nox3*^{eqlb} cells produced more ROS after 7 days *in vitro* (DIV), and significantly less after 12 DIV, when compared to BALB/c cells (Fig. 2g).

3.3. Cerebellar development is impaired in Nox3^{eqlb} mutant mice

Due to the deficit in motor coordination and balance observed in *Nox3*^{eqlb} (Fig. 1b), and the increased production of ROS by GCPs and NSCs *in vitro* (Fig. 2g), we decided to investigate if the cerebellum development was affected by the mutation. First, we measured the cerebellum of *Nox3*^{eqlb} and BALB/c adults (P45) and observed no differences in size (Fig. 3a). Additionally, we analyzed cerebellar cytoarchitecture and found that the external granular layer (EGL) of P15 *Nox3*^{eqlb} was thicker than BALB/c (Fig. 3b). Next, we evaluated the development of cerebellar Purkinje cells during a critical postnatal period, P6–P15.

Using parasagittal sections to localize Purkinje cells by immunostaining calbindin, we observed that the Purkinje cell monolayer was disorganized in *Nox3*^{eqlb} when compared to BALB/c at same ages (Fig. 3c). Thickening of the EGL could be due to decreased migration of GCPs out of the EGL, increased proliferation, decreased apoptosis, or a combination of these three factors. We first addressed if GCP migration was defective in *Nox3*^{eqlb}. To do so, we injected P5 mice with BrdU to label proliferating GCPs in the EGL, and euthanized the animals after 24–96 h, to evaluate GCP migration towards the internal granular layer (IGL). The analysis revealed that *Nox3*^{eqlb} GCP emigration from the EGL was similar to what was observed for BALB/c mice (Fig. 3d). Interestingly, we noticed that there were more BrdU$^+$ cells in the mutant mice when compared to BALB/c mice, suggesting increased proliferation (Fig. 3d). To determine if proliferation was indeed increased in *Nox3*^{eqlb}, organotypic cultures from P3-P15 mouse cerebella were labeled with [^{3}H]-thymidine. For all ages except P15, the proliferation rate was higher in *Nox3*^{eqlb} (Fig. 3e). Isolated P6 *Nox3*^{eqlb} GCPs also showed increased proliferation *in vitro*, indicating a cell-autonomous impairment of cell cycle control (Fig. 3e). We further investigated if increased proliferation also occurred in other cell types in *Nox3*^{eqlb}, starting with cerebellar NSCs. Neurospheres derived from *Nox3*^{eqlb} cerebellar NSCs increased in size earlier than their counterparts from

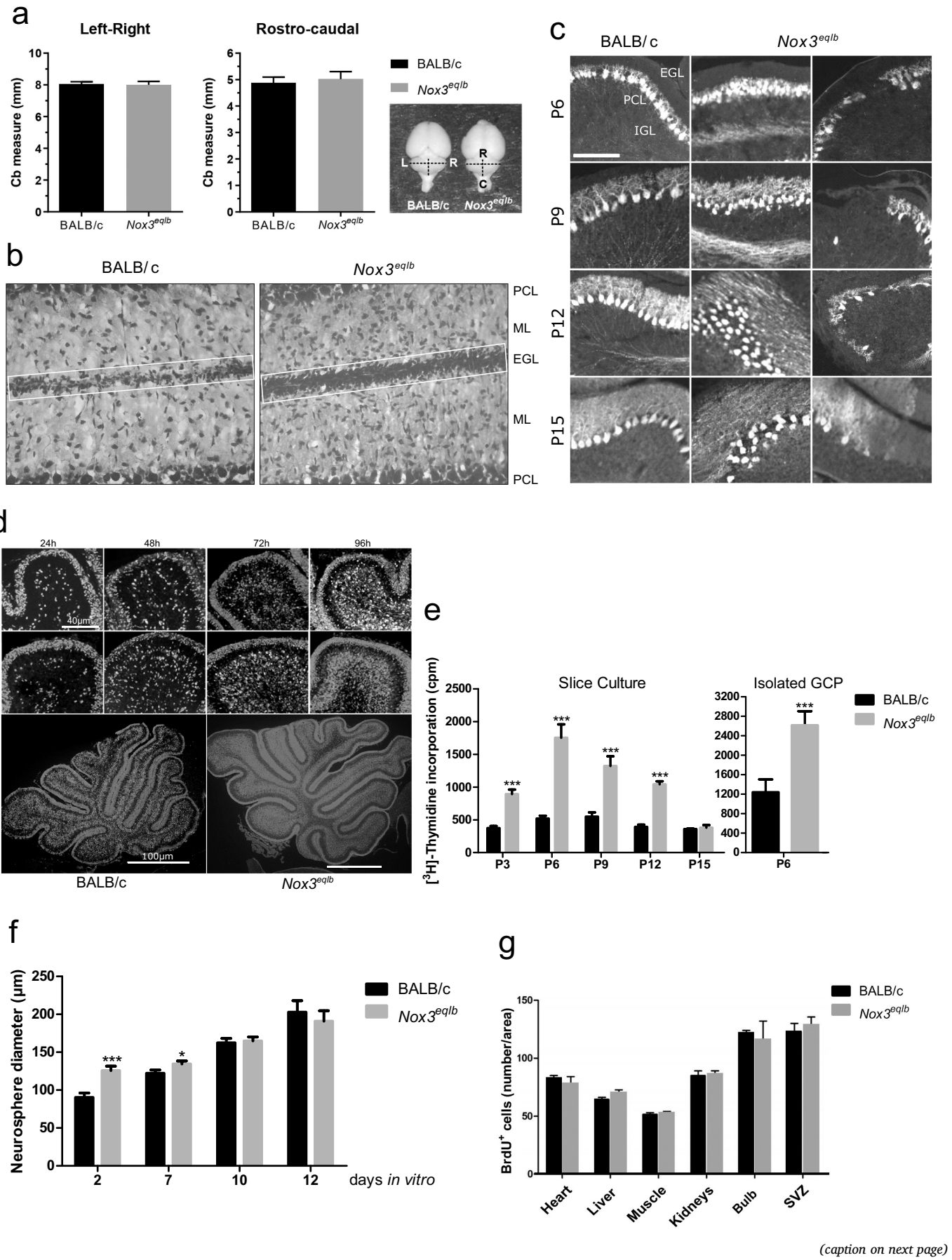

(caption on next page)

Fig. 3. *Nox3*^{eqlb} mutation disturbs neonatal cerebellar development.
(a) Measurement of left-right and rostro-caudal axis of cerebella from BALB/c (N = 20) and *Nox3*^{eqlb} (N = 22) adult (P45) mice shows no difference. On the right panel, image of whole adult mouse brain showing the axis used for the measurement.
(b) Nissl staining of P15 cerebellum shows larger and denser external granule cell (EGL) layer in *Nox3*^{eql}. PCL: Purkinje cell layer; ML: molecular layer. Scale bar = 40 μm.
(c) Calbindin immunostaining showing disrupted Purkinje cell development in *Nox3*^{eqlb}. IGL: internal granule cell layer. Scale bar = 40 μm.
(d) P5 mice were injected with BrdU to label proliferating cells *in vivo* and euthanized after 24–96 h to allow GCP emigration from the EGL. Upper panels: a *folium* was selected to show GCP emigration over time. Lower panels: whole cerebellum was photographed to show increased amount of BrdU$^+$ cells in *Nox3*^{eqlb} (right bottom panel) compared to BALB/c (left bottom panel).
(e) Proliferation was measured in slices of cerebellum from P3–P15 and isolated GCPs isolated from P6 mice. Representative data from one experiment repeated twice, in triplicates (***p < 0,0001).
(f) Neurospheres formed by cerebellar neural stem cell (NSCs) isolated at P6 were kept *in vitro* for 2–12 days. Diameter of the spheres was measured. N = 52 BALB/c neurospheres (2 days *in vitro*); N = 64 *Nox3*^{eqlb} neurospheres (2 days *in vitro*); N = 62 BALB/c neurospheres (7 days *in vitro*); N = 88 *Nox3*^{eqlb} neurospheres (7 days *in vitro*); N = 86 BALB/c neurospheres (10 days *in vitro*); N = 60 *Nox3*^{eqlb} neurospheres (10 days *in vitro*); N = 30 BALB/c neurospheres (12 days *in vitro*); N = 36 *Nox3*^{eqlb} neurospheres (12 days *in vitro*) (*p < 0.05; ***p < 0,0001).
(g) BrdU$^+$ cells in the heart, liver, muscle, kidneys, olfactory bulb and subventricular zone (SVZ) of P7 mice. No statistically significant differences were observed.

BALB/c (2–7 days *in vitro*), but reached the same size at day 10, suggesting that rapidly dividing stem cells are more affected than slowly dividing NSCs (Fig. 3f). Analysis of cell proliferation in other tissues and organs, as well as from different regions of the brain, showed no increased proliferation in *Nox3*^{eqlb} (Fig. 3g). *In vitro* inhibition of MAP kinase and PLC-γ by U0126 and U73122, respectively, did not decrease the proliferation rate of *Nox3*^{eqlb} GCPs, whereas both inhibited the proliferation of BALB/c GCPs (Supplementary Fig. 2).

We also investigated apoptosis in the developing cerebellum and found no differences between BALB/c and *Nox3*^{eqlb} (data not shown). Altogether, these results indicate that *Nox3*^{eqlb} GCPs have abnormal control of proliferation with no changes in migration or apoptosis.

3.4. *Nox3*^{eqlb} mutation causes altered expression of genes involved in the control of cell proliferation

cDNA microarray analysis of cerebella dissected from P6 and P15 revealed genes up and downregulated in *Nox3*^{eqlb} in comparison to their expression levels in BALB/c (Fig. 4a and Table 2). When we set a threshold at p = 0.05, we were able to limit the number of genes to 116 upregulated and 40 downregulated in *Nox3*^{eqlb} at P6 (Fig. 4b). As postnatal development progressed, we encountered 64 upregulated and 5 downregulated genes at P15. Functional *in silico* analysis of the differentially expressed transcripts at P6 revealed many connected genes that belong to networks related to proliferation and cell growth, neurological diseases, and the development and function of the nervous system (Fig. 4c and d).

Based on data showing increased proliferation and changes in gene expression at P6 and P15, we decided to quantify the expression of genes frequently involved in the control of cell proliferation, such as cyclins and cyclin-dependent kinases (cdks). Expression of *Cdkn2a* (cyclin-dependent kinase inhibitor 2A), a cell cycle arrest inducer, and *Cd133* was decreased in P6 *Nox3*^{eqlb} when compared to BALB/c. As expected, we found that genes involved in the progression of the cell cycle, such as *Ccnb1*, *Cdk1*, *Rb1*, *Cdc25*, *Akt1*, and *Sox2* were upregulated (Fig. 4e).

SHH, the main mitogen for GCPs during postnatal cerebellar development [3,19], is activated by ROS [20]. These data combined, with our results showing that inhibition of classic receptor tyrosine kinase pathways did not inhibit proliferation in *Nox3*^{eqlb} GCPs (Supplementary Fig. 2), led us to investigate if the SHH pathway was constitutively activated in *Nox3*^{eqlb} cerebellum. Quantification of SHH in the whole cerebellum showed increased concentration in *Nox3*^{eqlb} when compared to BALB/c (Fig. 5a). We quantified the expression of the transcription factors *Gli1*, *2*, and *3* by qPCR, and observed that all three genes were upregulated in the P6 *Nox3*^{eqlb} cerebellum when compared to BALB/c, as well as Cyclin D1 (*Ccnd1*), a target of SHH signaling [21] (Fig. 5b). These data suggest that increased proliferation of cerebellar GCPs in *Nox3*^{eqlb} mice is due to defective SHH signaling caused by excessive ROS production.

3.5. NOX inhibition decreases GCPs proliferation in vitro and in vivo

To obtain insight into the biological significance of the increased production of ROS by GCPs *in vivo*, we treated newborn pups daily with the NOX inhibitor apocynin (Apo) starting at P2 for 7 days and measured the thickness of the EGL at P9. The cerebella of both lineages, *Nox3*^{eqlb} and BALB/c, showed decreased thickness of the EGL, although the data did not show statistically significant differences between Apo-treated and untreated mice; the EGL of *Nox3*^{eqlb} mice treated with the NOX inhibitor for 7 days was the same size as in BALB/c mice (Fig. 5d, Supplementary Fig. 3).

As the increased proliferation of cerebellar GCPs and NSCs seemed to be a cell autonomous defect (Fig. 3e), we then evaluated if *in vitro* inhibition of NOX would affect proliferation. In fact, we observed decreased proliferation of GCPs and NSCs upon NOX inhibition (Fig. 5c). Upregulation of SHH pathway target expression, mainly *Gli* family members (Fig. 5b), led us to investigate if NOX inhibition would interfere with their expression. Indeed, NOX inhibition caused the upregulation of *Gli1* and *Gli3*, and the downregulation of *Gli2* and *Ccnd1* in both mouse lineages, *Nox3*^{eqlb} and BALB/c (Fig. 5e).

4. Discussion

NOX3 is a member of the NADPH oxidase family, and acts by reducing oxygen to superoxide ($O_2^{-}\cdot$) and other ROS. The involvement of ROS in the regulation of several cellular processes such as differentiation, migration, and cell death, has been reported in the literature [22–24]. In the present study, we describe a novel, unique mutation in Nox3 identified in an ENU-mutated BALB/c mouse (*Nox3*^{eqlb}). We mapped the mutation to position 934 of *Nox3*, an A to T transversion that resulted in p.Asn64Tyr substitution. To our knowledge, the mutation we describe here has not been described before, and is distinct from the described earlier by Paffenholz and colleagues [25].

These mutations in *Nox3* are illustrated in Supplementary Fig. 4. Although no mutation was found for the human homolog, an interesting description of four patients with a microdeletion in 6q25, which includes *NOX3*, was reported. Those patients have dysmorphic features, developmental disturbs, microcephaly and hearing loss [26].

We show here that *Nox3*^{eqlb} cerebellar GCPs and NSCs produce higher levels of H_2O_2 *in vitro* when compared to the cells isolated from BALB/c wild-type mice, and we postulate this to be the cause for increased proliferation observed *in vitro* and *in vivo* [18], as the inhibition of NOX *in vivo* reduced proliferation of GCPs to wild-type levels. Additionally, *Nox3*^{eqlb} GCPs and NSCs downregulated H_2O_2 production after 12 days *in vitro*, suggesting a preservative mechanism to protect cells from death by excess ROS [23]. We have not investigated if *Nox3*^{eqlb} cells activate ROS removal systems such as increased

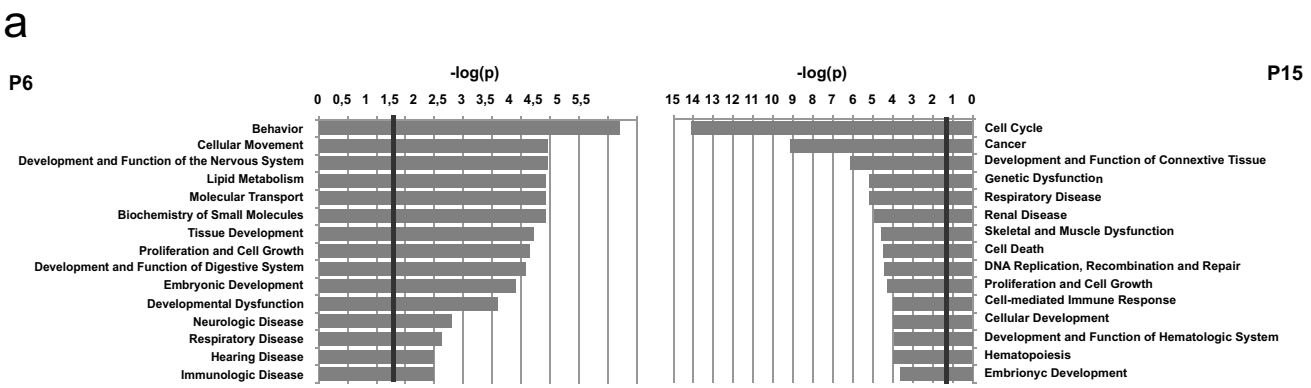

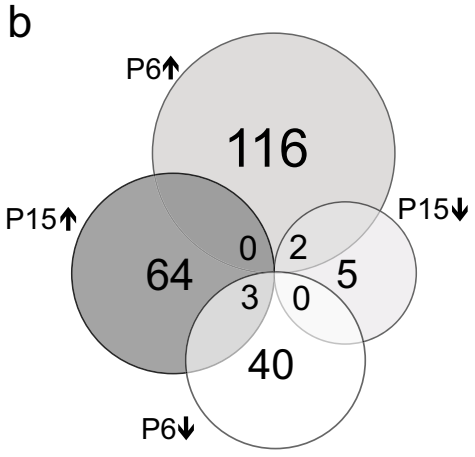

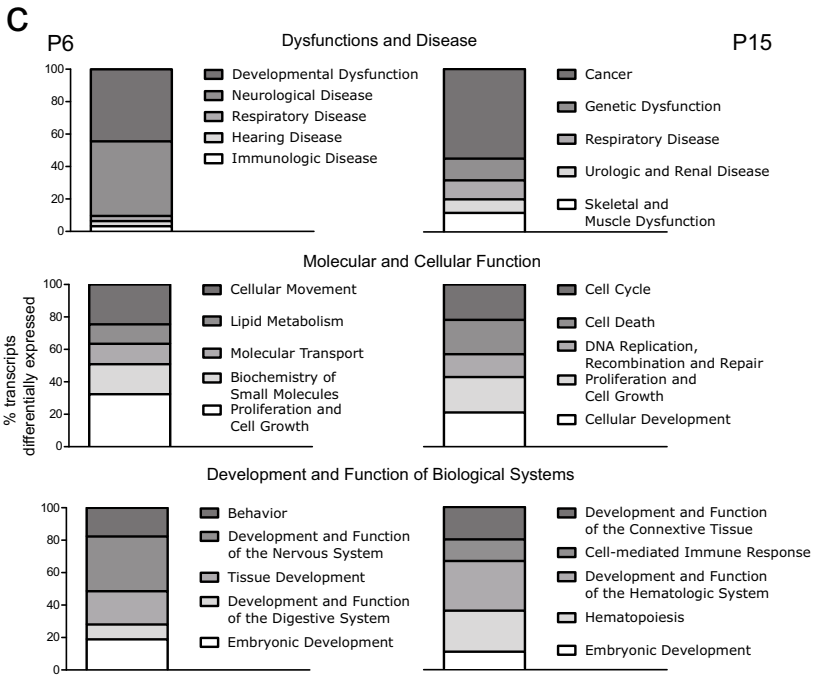

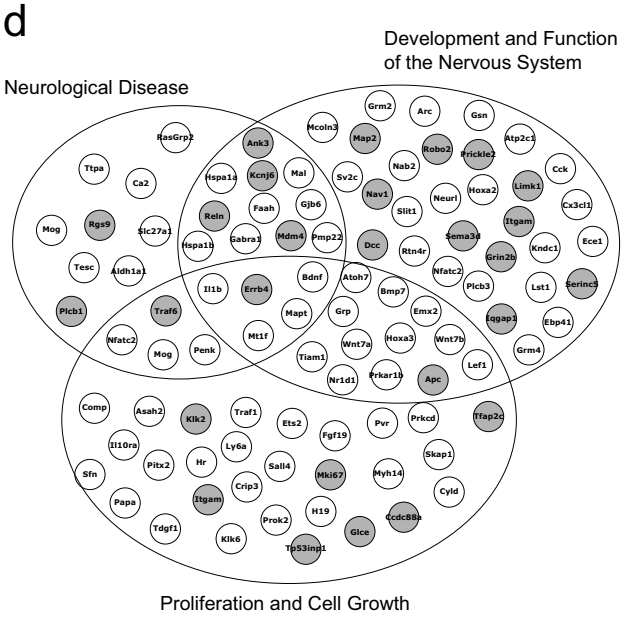

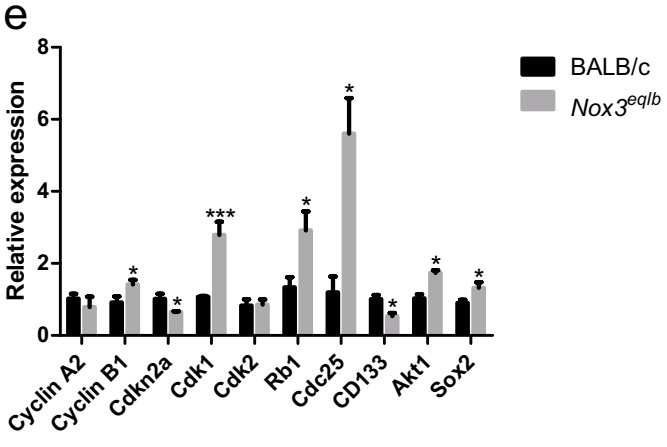

(caption on next page)

Fig. 4. Cerebellar gene expression is affected by *Nox3*^{eqlb} mutation.
(a) cDNA microarray shows groups of genes differentially expressed in P6 and P15 in *Nox3*^{eqlb} cerebellum when compared to BALB/c. Expression threshold was set to 1.30103 [− log(p) where p = 0.05] (vertical black line).
(b) Data from cDNA microarray were filtered at threshold and genes up and downregulated in P6 and P15 in *Nox3*^{eqlb} were clustered.
(c) Percentage of transcripts differentially expressed in P6 and P15 *Nox3*^{eqlb}.
(d) Networks related to proliferation and cell growth, neurological diseases, and development and function of the nervous system formed by genes differentially expressed by P6 *Nox3*^{eqlb}.
(e) Genes involved in the control of GCP and NSC proliferation expressed in P6 cerebellum. Data normalized by *Hprt*, *Actb* and *Rplp0* expression. N = 4 *Nox3*^{eqlb} cerebella; 5 BALB/c cerebella (*p < 0.05; ***p < 0.0001).

Table 2
Functional analysis of differentially expressed transcripts.

		n	p
Dysfunctions and diseases			
P6	Developmental dysfunction	28	7,96E − 04–4,56E − 02
	Neurological disease	29	5,06E − 03–4,22E − 02
	Respiratory disease	2	7,47E − 03–4,56E − 02
	Hearing disease	2	1,03E − 02–4,56E − 02
	Immunologic disease	2	1,03E − 02–4,56E − 02
P15	Cancer	33	7,76E − 10–3,98E − 02
	Genetic dysfunction	8	7,26E − 06–1,81E − 02
	Respiratory disease	7	7,26E − 06–3,59E − 02
	Renal and urologic disease	5	1,09E − 05–9,09E − 03
	Muscular and skeletal dysfunction	7	2,93E − 05–1,81E − 02
Molecular and cellular function			
P6	Cellular movement	41	1,10E − 04–4,56E − 02
	Lipid metabolism	20	1,17E − 04–4,56E − 02
	Molecular transport	21	1,17E − 04–4,56E − 02
	Biochemistry of small molecules	31	1,17E − 04–4,56E − 02
	Proliferation and cell growth	54	2,25E − 04–4,56E − 02
P15	Cell cycle	31	8,62E − 15–4,01E − 02
	Cell death	30	3,77E − 05–4,01E − 02
	DNA replication, recombination and repair	20	3,97E − 05–3,59E − 02
	Proliferation and cell growth	31	5,28E − 05–3,59E − 02
	Cellular development	30	1,20E − 04–3,96E − 02
Development and function of biological systems			
P6	Behavior	31	6,39E − 06–4,02E − 02
	Development and function of the nervous system	59	1,10E − 04–4,56E − 02
	Tissue development	36	1,94E − 04–4,56E − 02
	Development and function of the digestive system	16	2,68E − 04–4,56E − 02
	Embryonic development	33	3,97E − 04–4,56E − 02
P15	Development and function of connective tissue	15	7,92E − 07–4,01E − 02
	Cell-mediated immune response	10	1,20E − 04–3,59E − 02
	Development and function of the hematologic system	23	1,20E − 04–3,86E − 02
	Hematopoiesis	19	1,20E − 04–3,86E − 02
	Embryonic development	8	2,44E − 04–3,59E − 02

expression of catalase, superoxide dismutase (SOD), glutathione peroxidase and NRF2 [27]. The activation of anti-oxidant systems could be an explanation for the decreased production of H_2O_2 after long-term culture, which was not observed for wild-type cells.

Nox3^{eqlb} mice tested on the rotating bar showed significantly worse performance when compared to wild-type BALB/c mice, indicating that they present poor motor coordination, and this condition did not improve with training. Also, the phenotype did not worsen with age, suggesting it was not neurodegenerative. The cerebellar cytoarchitecture of *Nox3*^{eqlb} mutant mice showed a thicker EGL and, in several regions, Purkinje cells were either missing or disorganized. Using the Purkinje cell marker calbindin, we observed that the dendrite trees were defective, less numerous, and shorter in *Nox*^{eqlb} than in BALB/c. Degeneration of Purkinje cells has been related to ataxia in humans and in model mice [28–31], and animal models for ataxia-telangiectasia show defects in dendriogenesis in Purkinje cells caused by oxidative stress [32]. The lack of motor coordination observed in the *Nox3*^{eqlb} mutant mice could be explained by the misplacement and abnormal dendrite trees of Purkinje cells as well as by the excessive number of GCPs.

We concentrated on understanding why GCPs proliferate more in *Nox3*^{eqlb} than in BALB/c during postnatal development, and if an excess of ROS could participate in this process. We first investigated if the excess proliferation was a cell autonomous defect. Indeed, when *Nox3*^{eqlb} GCPs were cultured, either isolated or in organotypic slices, they proliferated more than GCPs from BALB/c mice. Similar results were observed for the growth of neurospheres generated from cerebellar NSCs. Cells were cultured in 10% FBS, which is rich in growth factors such as PDGF and FGF, and FGF is a known mitogen for GCPs [33]. In order to verify if the activation of receptor tyrosine kinases was responsible for the excess proliferation, we inhibited MAP kinase and PLC-γ. Neither inhibitor was effective in inhibiting *Nox3*^{eqlb} GCPs proliferation, although they were for BALB/c GCP, suggesting the activation was downstream of MAP kinase and/or other mitogens were involved. We already had an indication that excess ROS was involved, and it has been described for several cell types that ROS produced by NOX family members can activate proliferation [34].

In an attempt to identify target genes with up- or downregulated expression in *Nox3*^{eqlb} during early postnatal development, which could be informative regarding the observed phenotype, we performed a cDNA microarray using cerebella from P6 and P15 mice. One hundred and sixteen genes were upregulated in the P6 *Nox3*^{eqlb} cerebellum, whereas 40 were downregulated, when compared to BALB/c; the number of genes up- (64) and down- (5) regulated decreased as *Nox3*^{eqlb} mice aged. We found several target genes in which expression was affected by mutated *Nox3*, and many of them were related to proliferation, but we were not able to identify a pathway that stood out from the others, so we investigated the SHH signaling pathway. SHH is a morphogen known to regulate GCP proliferation during embryonic and postnatal development [1,4,35,36].

We describe here the upregulation of *Gli1*, *2*, and *3* in the *Nox3*^{eqlb} cerebellum, as well as the overexpression of *Ccnd1*, a main target of the SHH pathway. Overexpression of *Gli* and *Ccnd1* is closely related to increased GCP proliferation, and inhibition of SHH signaling significantly reduces the proliferation of GCPs [37]. Moreover, knockout mice for Cyclin D1 demonstrate a reduction in GCP proliferation and impaired cerebellar growth [38]. During development, aberrant activation of SHH causes alterations in cerebellar foliation, and this morphogen is highly involved in the formation of medulloblastoma, the most common malignant brain tumor in children arising during cerebellar development [19,22,36]. Some of the major factors involved in medulloblastoma initiation and progression are overproliferating SHH dependent-cerebellar GCPs and NSCs, and NOX-derived ROS acting on gene regulation [19,37,39–42]. We did not find tumors in the *Nox3*^{eqlb} cerebellum, possibly because medulloblastoma is caused by a combination of several somatic mutations, such as those described for human medulloblastoma: CTNNB1, PTCH1, MLL2, SMARCA4, TP53, DDX3X, GPS2, BCOR, and LDB1, among others [43]. High expression of *Cd133* is related to the formation of medulloblastoma [44], and our results showed downregulation of *Cd133* in *Nox3*^{eqlb}, which could explain the absence of tumors.

The investigation of the expression of genes involved in the control of cell cycle revealed the upregulation of several of them, such as *Ccnb1*, *Cdk1*, *Rb1*, *Cdc25*, and *Sox2* [45], and downregulation of other genes, such as *Cdkn2a* (p16^{INK4a}), the function of which is to inhibit G1/

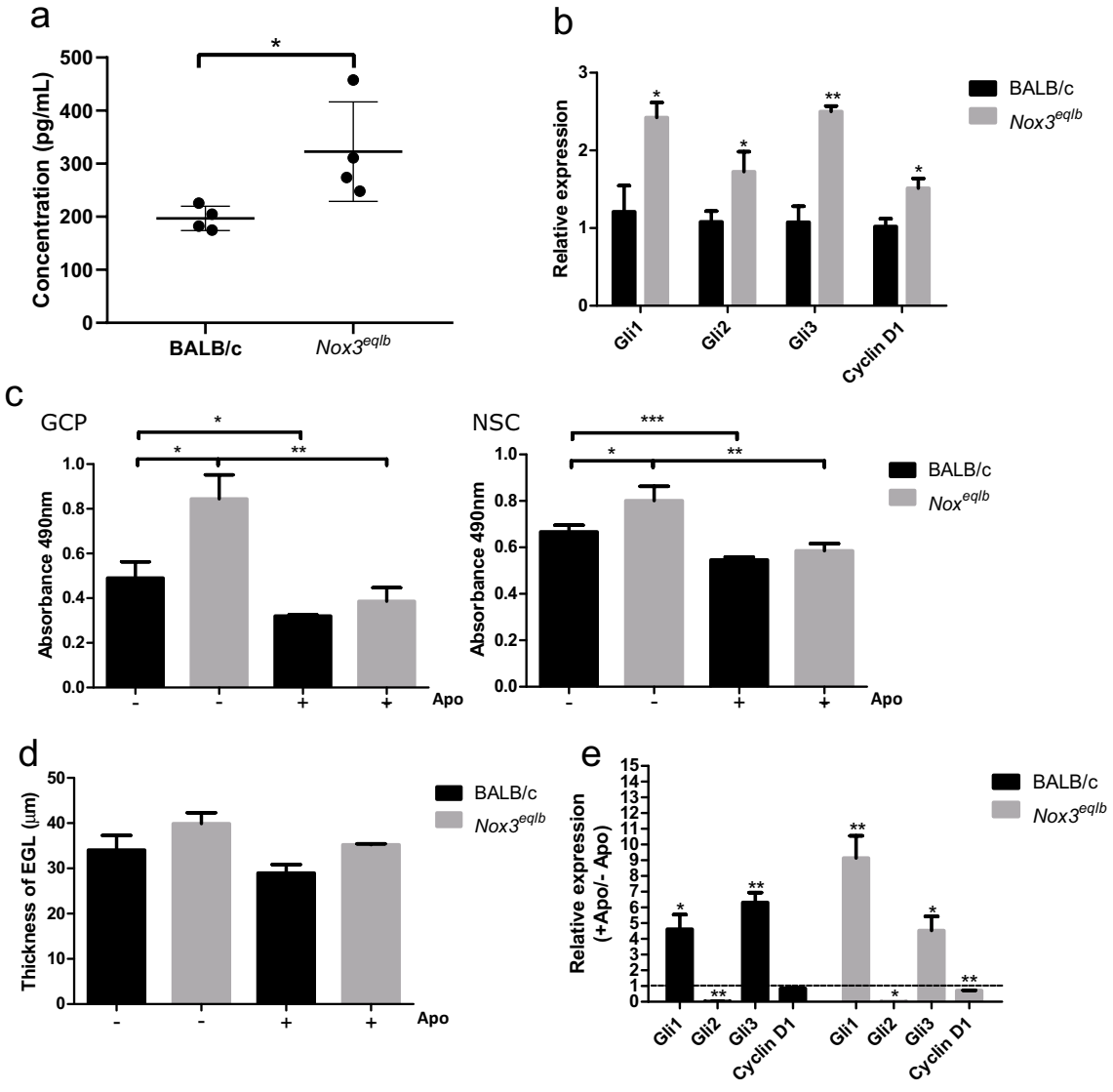

Fig. 5. Inhibition of NOX restores proliferation of *Nox3*^{eqlb} cells to BALB/c level.
(a) *Nox3*^{eqlb} cerebellum expresses more SHH compared to BALB/c. SHH was quantified by ELISA using protein extracted from the whole cerebellum of P6 mice. BALB/c and *Nox3*^{eqlb} N = 4 cerebella (*p < 0.05).
(b) qPCR analysis of *Glis* and Cyclin D1 (*Ccnd1*) expression in P6 cerebellum shows increased expression in *Gli1–3* and Cyclin D1 in *Nox3*^{eqlb}. Data normalized by *Hprt*, *Actb* and *Rplp0* expression. N = 5 BALB/c cerebella; 3 *Nox3*^{eqlb} cerebella (*p < 0.05; **p < 0.01).
(c) *In vitro* proliferation assay after treatment with 100 µM apocynin (Apo) or DMSO for 24 h. GCPs: N = 10 wells for BALB/c and 11 wells for Nox3^{eqlb}; NSCs: N = 11 wells for BALB/c and 11 wells for *Nox3*^{eqlb} (*p < 0.05; **p < 0.01; ***p < 0.0001 compared to the control).
(d) Measurement of EGL showing reduction of cerebellar EGL thickness of BALB/c and *Nox3*^{eqlb} mice after treatment with 10 µg/g apocynin. BALB/c N = 4; *Nox3*^{eqlb} N = 5; BALB/c + APO N = 6; *Nox3*^{eqlb} + APO N = 4.
(e) qPCR analysis of the expression of *Gli1–3* and Cyclin D1 (*Ccnd1*) in P6 cerebellum after apocynin treatment. Data normalized by *Hprt*, *Actb* and *Rplp0* expression. N = 3 BALB/c cerebella; 5 *Nox3*^{eqlb} cerebella (*p < 0.05; **p < 0.01).

S transition, causing cell cycle arrest. Low expression or total loss of *Cdkn2a* promotes increased proliferation in GCPs induced by SHH [46]. Akt1 (protein kinase B), a member of the serine/threonine kinase family, also participates in G1/S transition and can control the expression or activity of cyclins D1 and B1, in addition to inhibitors of the cyclin-dependent kinases Cdkn1a and 1b [47]. *Akt1* is a transcriptional target of Gli, and expression increases after activation of the HH pathway[48] (hedgehog, the human SHH analogue); we found that Akt1 was upregulated in *Nox3*^{eqlb} mice.

In order to understand if excess NOX-produced ROS was the basis for disrupted SHH signaling, we inhibited NOX activity with apocynin [22,49], and observed a reduction in *Nox3*^{eqlb} and BALB/c GCP and NSC proliferation. Previous reports have demonstrated that ROS is a second messenger in signaling pathways for neural/progenitor cell proliferation [18,24]. We also verified that *in vivo* expression of *Gli2* and Cyclin D1 (*Ccnd1*) was downregulated, whereas *Gli1* and *Gli3* expression was upregulated after apocynin treatment in both mouse lineages. Gli2 is the main activator/mediator of the SHH pathway in the control of GCP proliferation, and it directly regulates the transcription of cell cycle-regulated genes such as Cyclin D1 [35,50]. Gli3 is predominantly a repressor of SHH signaling, and may induce Gli1 expression [51]. We suggest that Gli2 may be the direct regulator of SHH signaling and the main regulator of *Ccnd1* expression in *Nox3*^{eqlb}. Gli3 may act as a Gli2 compensator and as a direct promoter of Gli1 [52].

In conclusion, our results demonstrate that ROS acts as a second messenger in the control of cerebellar GCP proliferation, and that NOX

inhibition reverses the excessive proliferation phenotype, indicating that the increased proliferation rate observed in *Nox3*^{eqlb} is intimately associated with NOX-derived ROS.

Supplementary data to this article can be found online at https://doi.org/10.1016/j.bbadis.2019.02.022.

Transparency document

The Transparency document associated with this article can be found, in online version.

Acknowledgements

This work was funded by FAPESP (grants 2017/18765-4 to M.A.P. and 2012/25387-2 to C.F.M.M.; and fellowships 2014/19204-8 to P.C.M., 2018/05635-8 to S.G.O.), CNPq (fellowship 14411/2017-1 to T.A.S.), and Coordenação de Aperfeiçoamento de Pessoal de Nível Superior – CAPES (Finance Code 001). We thank the Core Facility for Scientific Research – University of Sao Paulo (CEFAP-USP/GENIAL) for NGS sequencing.

References

[1] K. Leto, M. Arancillo, E.B. Becker, A. Buffo, C. Chiang, B. Ding, W.B. Dobyns, I. Dusart, P. Haldipur, M.E. Hatten, M. Hoshino, A.L. Joyner, M. Kano, D.L. Kilpatrick, N. Koibuchi, S. Marino, S. Martinez, K.J. Millen, T.O. Millner, T. Miyata, E. Parmigiani, K. Schilling, G. Sekerková, R.V. Sillitoe, C. Sotelo, N. Uesaka, A. Wefers, R.J. Wingate, R. Hawkes, Consensus paper: cerebellar development, Cerebellum 15 (6) (2016) 789–828.

[2] H.J. Ten Donkelaar, M. Lammens, Development of the human cerebellum and its disorders, Clin. Perinatol. 36 (3) (2009) 513–530.

[3] R.J. Wechsler-Reya, M.P. Scott, Control of neuronal precursor proliferation in the cerebellum by Sonic Hedgehog, Neuron 22 (1) (1999) 103–114.

[4] C. Vaillant, D. Monard, SHH pathway and cerebellar development, Cerebellum 8 (3) (2009) 291–301.

[5] M.S. Salman, Epidemiology of cerebellar diseases and therapeutic approaches, Cerebellum. (2018) 4–11, https://doi.org/10.1007/s12311-017-0885-2.

[6] J.P. Flaherty, H.E. Fairfield, C.A. Spruce, C.M. McCarty, D.E. Bergstrom, Molecular characterization of an allelic series of mutations in the mouse Nox3 gene, Mamm. Genome 22 (3–4) (2011) 156–169.

[7] S.M. Massironi, B.L. Reis, J.G. Carneiro, L.B. Barbosa, C.B. Ariza, G.C. Santos, J.L. Guénet, A.L. Godard, Inducing mutations in the mouse genome with the chemical mutagen ethylnitrosourea, Braz. J. Med. Biol. Res. 39 (9) (2006) 1217–1226.

[8] H. Fairfield, G.J. Gilbert, M. Barter, R.R. Corrigan, M. Curtain, Y. Ding, M. D'Ascenzo, D.J. Gerhardt, C. He, W. Huang, T. Richmond, L. Rowe, F.J. Probst, D.E. Bergstrom, S.A. Murray, C. Bult, J. Richardson, B.T. Kile, I. Gut, J. Hager, S. Sigurdsson, E. Mauceli, F. Di Palma, K. Lindblad-Toh, M.L. Cunningham, T.C. Cox, M.J. Justice, M.S. Spector, S.W. Lowe, T. Albert, L.R. Donahue, J. Jeddeloh, J. Shendure, L.G. Reinholdt, Mutation discovery in mice by whole exome sequencing, Genome Biol. 12 (9) (2011) R86.

[9] A. Cox, C.L. Ackert-Bicknell, B.L. Dumont, Y. Ding, J.T. Bell, G.A. Brockmann, J.E. Wergedal, C. Bult, B. Paigen, J. Flint, S.W. Tsaih, G.A. Churchill, K.W. Broman, A new standard genetic map for the laboratory mouse, Genetics 182 (4) (2009) 1335–1344.

[10] P. Danecek, A. Auton, G. Abecasis, C.A. Albers, E. Banks, M.A. DePristo, R.E. Handsaker, G. Lunter, G.T. Marth, S.T. Sherry, G. McVean, R. Durbin, G. P. A. Group, The variant call format and VCFtools, Bioinformatics 27 (15) (2011) 2156–2158.

[11] K. Wang, M. Li, H. Hakonarson, ANNOVAR: functional annotation of genetic variants from high-throughput sequencing data, Nucleic Acids Res. 38 (16) (2010) e164.

[12] Y. Choi, G.E. Sims, S. Murphy, J.R. Miller, A.P. Chan, Predicting the functional effect of amino acid substitutions and indels, PLoS One 7 (10) (2012) e46688.

[13] I.A. Adzhubei, S. Schmidt, L. Peshkin, V.E. Ramensky, A. Gerasimova, P. Bork, A.S. Kondrashov, S.R. Sunyaev, A method and server for predicting damaging missense mutations, Nat. Methods 7 (4) (2010) 248–249.

[14] M.A. Porcionatto, C.R. Moreira, C.F. Lotfi, H.A. Armelin, C.P. Dietrich, H.B. Nader, Stimulation of heparan sulfate proteoglycan synthesis and secretion during G1 phase induced by growth factors and PMA, J. Cell. Biochem. 70 (4) (1998) 563–572.

[15] A.P. Araujo, M.E. Ribeiro, R. Ricci, R.J. Torquato, L. Toma, M.A. Porcionatto, Glial cells modulate heparan sulfate proteoglycan (HSPG) expression by neuronal precursors during early postnatal cerebellar development, Int. J. Dev. Neurosci. 28 (7) (2010) 611–620.

[16] M. Zusso, P. Debetto, Isolation and culture of neural progenitor cells from rat postnatal cerebellum, Methods Mol. Biol. 846 (2012) 39–47.

[17] K.J. Livak, T.D. Schmittgen, Analysis of relative gene expression data using real-time quantitative PCR and the 2(−Delta Delta C(T)) Method, Methods 25 (4) (2001) 402–408.

[18] J.E. Le Belle, N.M. Orozco, A.A. Paucar, J.P. Saxe, J. Mottahedeh, A.D. Pyle, H. Wu, H.I. Kornblum, Proliferative neural stem cells have high endogenous ROS levels that regulate self-renewal and neurogenesis in a PI3K/Akt-dependant manner, Cell Stem Cell 8 (1) (2011) 59–71.

[19] N. Dahmane, A. Ruiz i Altaba, Sonic hedgehog regulates the growth and patterning of the cerebellum, Development 126 (14) (1999) 3089–3100.

[20] R.L. Dai, S.Y. Zhu, Y.P. Xia, L. Mao, Y.W. Mei, Y.F. Yao, Y.M. Xue, B. Hu, Sonic hedgehog protects cortical neurons against oxidative stress, Neurochem. Res. 36 (1) (2011) 67–75.

[21] A.M. Kenney, D.H. Rowitch, Sonic hedgehog promotes G(1) cyclin expression and sustained cell cycle progression in mammalian neuronal precursors, Mol. Cell. Biol. 20 (23) (2000) 9055–9067.

[22] A. Coyoy, M. Olguín-Albuerne, P. Martínez-Briseño, J. Morán, Role of reactive oxygen species and NADPH-oxidase in the development of rat cerebellum, Neurochem. Int. 62 (7) (2013) 998–1011.

[23] M. Olguín-Albuerne, J. Morán, ROS produced by NOX2 control in vitro development of cerebellar granule neurons development, ASN Neuro 7 (2) (2015).

[24] M. Yoneyama, K. Kawada, Y. Gotoh, T. Shiba, K. Ogita, Endogenous reactive oxygen species are essential for proliferation of neural stem/progenitor cells, Neurochem. Int. 56 (6–7) (2010) 740–746.

[25] R. Paffenholz, R.A. Bergstrom, F. Pasutto, P. Wabnitz, R.J. Munroe, W. Jagla, U. Heinzmann, A. Marquardt, A. Bareiss, J. Laufs, A. Russ, G. Stumm, J.C. Schimenti, D.E. Bergstrom, Vestibular defects in head-tilt mice result from mutations in Nox3, encoding an NADPH oxidase, Genes Dev. 18 (5) (2004) 486–491.

[26] S.C. Nagamani, A. Erez, C. Eng, Z. Ou, C. Chinault, L. Workman, J. Coldwell, P. Stankiewicz, A. Patel, J.R. Lupski, S.W. Cheung, Interstitial deletion of 6q25.2-q25.3: a novel microdeletion syndrome associated with microcephaly, developmental delay, dysmorphic features and hearing loss, Eur. J. Hum. Genet. 17 (5) (2009) 573–581.

[27] C. Gorrini, I.S. Harris, T.W. Mak, Modulation of oxidative stress as an anticancer strategy, Nat. Rev. Drug Discov. 12 (12) (2013) 931–947.

[28] C.S. Duchala, H.E. Shick, J. Garcia, D.M. Deweese, X. Sun, V.J. Stewart, W.B. Macklin, The toppler mouse: a novel mutant exhibiting loss of Purkinje cells, J. Comp. Neurol. 476 (2) (2004) 113–129.

[29] Y. He, T. Zu, K.A. Benzow, H.T. Orr, H.B. Clark, M.D. Koob, Targeted deletion of a single Sca8 ataxia locus allele in mice causes abnormal gait, progressive loss of motor coordination, and Purkinje cell dendritic deficits, J. Neurosci. 26 (39) (2006) 9975–9982.

[30] S.I. Levin, Z.M. Khaliq, T.K. Aman, T.M. Grieco, J.A. Kearney, I.M. Raman, M.H. Meisler, Impaired motor function in mice with cell-specific knockout of sodium channel Scn8a (NaV1.6) in cerebellar purkinje neurons and granule cells, J. Neurophysiol. 96 (2) (2006) 785–793.

[31] J.T. Walter, K. Alviña, M.D. Womack, C. Chevez, K. Khodakhah, Decreases in the precision of Purkinje cell pacemaking cause cerebellar dysfunction and ataxia, Nat. Neurosci. 9 (3) (2006) 389–397.

[32] P. Chen, C. Peng, J. Luff, K. Spring, D. Watters, S. Bottle, S. Furuya, M.F. Lavin, Oxidative stress is responsible for deficient survival and dendritogenesis in purkinje neurons from ataxia-telangiectasia mutated mutant mice, J. Neurosci. 23 (36) (2003) 11453–11460.

[33] K. Müller Smith, T.L. Williamson, M.L. Schwartz, F.M. Vaccarino, Impaired motor coordination and disrupted cerebellar architecture in Fgfr1 and Fgfr2 double knockout mice, Brain Res. 1460 (2012) 12–24.

[34] K. Bedard, K.H. Krause, The NOX family of ROS-generating NADPH oxidases: physiology and pathophysiology, Physiol. Rev. 87 (1) (2007) 245–313.

[35] J.D. Corrales, G.L. Rocco, S. Blaess, Q. Guo, A.L. Joyner, Spatial pattern of sonic hedgehog signaling through Gli genes during cerebellum development, Development 131 (22) (2004) 5581–5590.

[36] P.M. Lewis, A. Gritli-Linde, R. Smeyne, A. Kottmann, A.P. McMahon, Sonic hedgehog signaling is required for expansion of granule neuron precursors and patterning of the mouse cerebellum, Dev. Biol. 270 (2) (2004) 393–410.

[37] Y. Men, A. Zhang, H. Li, Y. Jin, X. Sun, J. Gao, LKB1 regulates cerebellar development by controlling sonic hedgehog-mediated granule cell precursor proliferation and granule cell migration, Sci. Rep. 5 (2015) 16232.

[38] J. Pogoriler, K. Millen, M. Utset, W. Du, Loss of cyclin D1 impairs cerebellar development and suppresses medulloblastoma formation, Development 133 (19) (2006) 3929–3937.

[39] F. Mille, L. Tamayo-Orrego, M. Lévesque, M. Remke, A. Korshunov, J. Cardin, N. Bouchard, L. Izzi, M. Kool, P.A. Northcott, M.D. Taylor, S.M. Pfister, F. Charron, The Shh receptor Boc promotes progression of early medulloblastoma to advanced tumors, Dev. Cell 31 (1) (2014) 34–47.

[40] X. Shi, Y. Zhang, J. Zheng, J. Pan, Reactive oxygen species in cancer stem cells, Antioxid. Redox Signal. 16 (11) (2012) 1215–1228.

[41] F.J. Swartling, V. Savov, A.I. Persson, J. Chen, C.S. Hackett, P.A. Northcott, M.R. Grimmer, J. Lau, L. Chesler, A. Perry, J.J. Phillips, M.D. Taylor, W.A. Weiss, Distinct neural stem cell populations give rise to disparate brain tumors in response to N-MYC, Cancer Cell 21 (5) (2012) 601–613.

[42] D. Trachootham, J. Alexandre, P. Huang, Targeting cancer cells by ROS-mediated mechanisms: a radical therapeutic approach? Nat. Rev. Drug Discov. 8 (7) (2009) 579–591.

[43] T.J. Pugh, S.D. Weeraratne, T.C. Archer, D.A. Pomeranz Krummel, D. Auclair, J. Bochicchio, M.O. Carneiro, S.L. Carter, K. Cibulskis, R.L. Erlich, H. Greulich, M.S. Lawrence, N.J. Lennon, A. McKenna, J. Meldrim, A.H. Ramos, M.G. Ross, C. Russ, E. Shefler, A. Sivachenko, B. Sogoloff, P. Stojanov, P. Tamayo, J.P. Mesirov, V. Amani, N. Teider, S. Sengupta, J.P. Francois, P.A. Northcott, M.D. Taylor, F. Yu, G.R. Crabtree, A.G. Kautzman, S.B. Gabriel, G. Getz, N. Jäger, D.T. Jones, P. Lichter,

S.M. Pfister, T.M. Roberts, M. Meyerson, S.L. Pomeroy, Y.J. Cho, Medulloblastoma exome sequencing uncovers subtype-specific somatic mutations, Nature 488 (7409) (2012) 106–110.
[44] B. Manoranjan, C. Venugopal, N. McFarlane, B.W. Doble, S.E. Dunn, K. Scheinemann, S.K. Singh, Medulloblastoma stem cells: where development and cancer cross pathways, Pediatr. Res. 71 (4) (2012) 516–522 Pt 2.
[45] J. Ahlfeld, R. Favaro, P. Pagella, H.A. Kretzschmar, S. Nicolis, U. Schüller, Sox2 requirement in sonic hedgehog-associated medulloblastoma, Cancer Res. 73 (12) (2013) 3796–3807.
[46] S.W. Bruggeman, M.E. Valk-Lingbeek, P.P. van der Stoop, J.J. Jacobs, K. Kieboom, E. Tanger, D. Hulsman, C. Leung, Y. Arsenijevic, S. Marino, M. van Lohuizen, Ink4a and Arf differentially affect cell proliferation and neural stem cell self-renewal in Bmi1-deficient mice, Genes Dev. 19 (12) (2005) 1438–1443.
[47] M.V. Jain, A. Shareef, W. Likus, A. Cieślar-Pobuda, S. Ghavami, M.J. Łos, Inhibition of miR301 enhances Akt-mediated cell proliferation by accumulation of PTEN in nucleus and its effects on cell-cycle regulatory proteins, Oncotarget 7 (15) (2016) 20953–20965.
[48] N.K. Agarwal, C. Qu, K. Kunkalla, K. Kunkulla, Y. Liu, F. Vega, Transcriptional regulation of serine/threonine protein kinase (AKT) genes by glioma-associated oncogene homolog 1, J. Biol. Chem. 288 (21) (2013) 15390–15401.
[49] J. Stolk, T.J. Hiltermann, J.H. Dijkman, A.J. Verhoeven, Characteristics of the inhibition of NADPH oxidase activation in neutrophils by apocynin, a methoxy-substituted catechol, Am. J. Respir. Cell Mol. Biol. 11 (1) (1994) 95–102.
[50] J.J. White, R.V. Sillitoe, Development of the cerebellum: from gene expression patterns to circuit maps, Wiley Interdiscip. Rev. Dev. Biol. 2 (1) (2013) 149–164.
[51] C.B. Bai, D. Stephen, A.L. Joyner, All mouse ventral spinal cord patterning by hedgehog is Gli dependent and involves an activator function of Gli3, Dev. Cell 6 (1) (2004) 103–115.
[52] P. Dai, H. Akimaru, Y. Tanaka, T. Maekawa, M. Nakafuku, S. Ishii, Sonic hedgehog-induced activation of the Gli1 promoter is mediated by GLI3, J. Biol. Chem. 274 (12) (1999) 8143–8152.
[53] P. Kumar, S. Henikoff, P.C. Ng, Predicting the effects of coding non-synonymous variants on protein function using the SIFT algorithm, Nat. Protoc. 4 (7) (2009) 1073–1081, https://doi.org/10.1038/nprot.2009.86 (Epub 2009 Jun 25).
[54] D.B. Allison, X. Cui, G.P. Page, M. Sabripour, Microarray data analysis: from disarray to consolidation and consensus, Nat Rev Genet 7 (1) (2006) 55–65 (Review).